Development of Non-fluorinated Hybrid Ester Solvents for Wide-Temperature Operation of Lithium-Ion Batteries

Soung Jin Yang,[1†] Seungyeop Kang,[1†] Joo-Hyun Koo,[2] Gil-Ju Lee,[2] Seung-Gyu Lim,[2] Joo-Seong Kim,[2] Kyoungsuk Jin,[3] Hyun Woo Kim,[4,6] Hana Yoon,[5] and Dong-Joo Yoo[1]*

[1] School of Mechanical Engineering, Korea University, 145 Anam-ro, Seongbuk-gu, Seoul 02841, Republic of Korea

[2] LiBEST Inc., 34 Gukjegwahak 21-ro, Yuseong-gu, Daejeon 34002, Republic of Korea

[3] Department of Chemistry, Korea University, 145 Anam-ro, Seongbuk-gu, Seoul 02841, Republic of Korea

[4] Research Center for Materials Analysis, Korea Basic Science Institute (KBSI), Daejeon 34133, Republic of Korea

[5] Energy Storage Research Department, Korea Institute of Energy Research (KIER), Daejeon 34129, Republic of Korea

[6] Department of Chemical Engineering, Gyeongsang National University, Jinju 52828, Republic of Korea

*Email: djyoo@korea.ac.kr

Supporting Information.

Experimental Methods:

Electrolyte and Electrode Preparation:

Methyl 3-methoxypropionate (MMP), 2-methoxyethyl acetate (MEA), bis(trifluoromethane)sulfonimide lithium salt (LiTFSI) were purchased from Sigma-Aldrich. Fluoroethylene carbonate (FEC) was purchased from Chunbo. Ref electrolyte was prepared by purchasing 1M $LiPF_6$ in EC/DEC (v/v=1/1) electrolyte from Enchem and adding 5 wt% FEC additive. All solvents used were dried with 4 Å molecular sieves for a week before use. Electrolyte was made within argon-filled glovebox with oxygen and moisture levels below 1 ppm. All electrodes were provided by LiBEST. Anodes were composed of 90 wt% artificial graphite, 2 wt% conducting agent, and 8 wt% PVDF cased on copper foil. Cathodes were composed of 94 wt% $LiNi_{0.8}Mn_{0.1}Co_{0.1}O_2$ (NCM811), 3 wt% PVDF, and 3 wt% conducting agent casted on aluminum foil. Celgard 3501 was used as a separator. The diameters of anode, cathode and separators were 14 mm, 12.95 mm and 18 mm, respectively. The N/P ratio for electrochemical evaluations was matched at 1.04.

Electrochemical Measurements and Characterization:

Coin-type cells (CR2032, Welcos) were assembled within an argon-filled gloxbox with oxygen and moisture levels below 1 ppm. All the galvanostatic cycling was conducted by employing Wonatech WBCS3000 Cycler at various temperatures. The electrochemical impedance spectroscopy (EIS) was measured by employing Wonatech MP1 at room temperature. Galvano-EIS was utilized to measure the cell impedance after 5 formation cycles and charged at 3.7 V at

the frequency range of 1 MHz to 0.5 Hz and at an amplitude of 15% of the cell's capacity. EIS fitting was performed with ZMAN software. Ionic conductivity of each electrolyte was measured by using SUS||SUS cells. 14 mm outer 11 mm inner diameter PTFE donut at 2.1 mm height was glued onto the case, and 280 µL of electrolyte was poured within the donut. Potentio-EIS was utilized at various temperatures and the frequency range of 100 kHz to 0.1 Hz at an amplitude of 10 mV. The ionic conductivity was calculated with the equation given below:

$$Ionic\ Conductivity\left(\frac{mS}{cm}\right) = \frac{Height\ of\ PTFE(cm)}{Rs\ (\Omega) * Area\ (cm^2)} * 1000$$

The cycled cells were disassembled in an argon-filled glovebox at fully discharged state (2.8 V). Electrodes were rinsed with DEC for Ref cycled electrodes, MEA for MEA-TFSI cycled electrodes, and MMP for MMP-TFSI cycled electrodes. X-ray photoelectron spectroscopy (XPS, ESCALAB-250, Thermo Scientific) analysis was conducted using Al K alpha radiation. Field emission scanning electron microscopy (FE-SEM, JEOL JSM-700F) with accelerating voltage of 10 kV was utilized.

Computational Simulation:

Classical molecular dynamics (cMD) simulations were performed using LAMMPS software. The OPLS-AA force field [1] was applied to all solvents, while references by Jensen and Jorgensen,[2] Doherty,[3] and Gouveia[4] were used for Li^+, PF_6^- and $TFSI^-$, respectively. Atomic partial charges were derived by fitting to the molecular electrostatic potential at the atomic centers, using the B3LYP/aug-cc-pVDZ basis set.[5, 6] The number of molecules was adjusted to match the electrolyte compositions used in the experiments: 1) 562 EC/310 DEC/46 FEC/75 $LiPF_6^-$, 2) 577 MEA/105 FEC/75 LiTFSI, 3) 577 MMP/105 FEC/75 LiTFSI. Initially, molecules were randomly placed in

an 80x80x80Å box using the packing optimization for MD simulations (Packmol) program,[7] and the systems were stabilized to approximately 50x50x50Å. All systems were defined with periodic boundary conditions and non-bonded interactions using the Lennard-Jones potential and Coulombic interactions with a cut-off distance of 1.2 nm. Additionally, the Particle-Particle Particle-Mesh (PPPM) method was applied to account for long-range Coulomb interactions. Each system underwent initial minimization at 0 K with a tolerance of 10^{-5} for both energy and force. To analyze the changes in solvation structure at various temperatures, after minimization, 12 systems were equilibrated at temperatures of 243.15 K, 263.15 K, 298.15 K, and 318.15 K, under a pressure of 1 atm.

Each system was equilibrated at the specified temperatures and 1 atm pressure in the NPT ensemble using a Parrinello-Rahman barostat for a duration of 2 ns. To prevent reaching a meta-stable state, the temperature was gradually increased to 500.15 K and then subsequently decreased back to the target temperatures through an annealing process, applying the NVT ensemble for 1.5 ns. After the annealing process, an NPT ensemble was applied for 4 ns to achieve equilibrium at constant temperature and pressure. Volume and energy values were recorded every 0.001 ns to monitor fluctuations and assess whether the system had reached a stable equilibrium state. In each system that reached equilibrium, NVT simulation was performed for 8.5 ns, during which the mean squared displacement (MSD), radial distribution function (RDF), and solvation structure were analyzed. The analysis of the MSD and solvation structure was conducted using the results obtained at 298.15 K. The MSD was obtained every 0.001 ns over the course of 8.5 ns, and the diffusivity and transference number were calculated using the equation given below:

$$D_{ion} = \lim_{t\to\infty} \frac{MSD(t)}{6t}, \quad t_{Li^+} = \frac{D_{Li^+}}{D_{Li^+} + D_{PF_6^- \text{ or } TFSI^-}}$$

The RDF was obtained every 0.01 ns during the 7 ns following the initial 1.5 ns of NVT simulation, which allowed for the calculation of the averaged RDF. The solvation shell was analyzed over a period of 7 ns, corresponding to the same interval as the averaged RDF, using trajectory files obtained every 0.01 ns. The probability density of the solvation structure type was calculated by considering the peaks of the solvent and anion within the first solvation sheath in the RDF. Thus, the solvation radius was set to 2.2 Å, which encompasses all peaks of each electrolyte. Snapshots of each system were visualized using Visual Molecular Dynamics (VMD) at 15 ns, emphasizing the solvation structures obtained through solvation shell analysis. The representative solvation structure resulted from geometry optimization was performed at the B3LYP/6-311+G(d,p) level, which provided the Li^+-O interatomic distance values.

All density functional theory (DFT) calculations were performed using Gaussian 16 software. The geometries of the solvent, ion, and ion-complex were optimized at the B3LYP/6-311G+(d) level,[8 9] and their stability was confirmed through frequency calculations. In the gas phase, these optimized structures were utilized to calculate the electrostatic potential (ESP), binding energies, and HOMO/LUMO energies. For the calculation of solvation energy, all solvation structures were extracted from the trajectory files of MD simulations, and structural optimization was carried out at the 6-311G+(d,p) level. To consider solvation effects, the SMD implicit solvent model[10] was used, with acetone as the explicit solvent (Eps = 20.493000, Eps(inf) = 1.846337). The solvation energy was calculated as the difference between the free energy of the solvated Li^+ complex and the sum of the free energies for the individual components: Li^+, the solvent, and the anion.

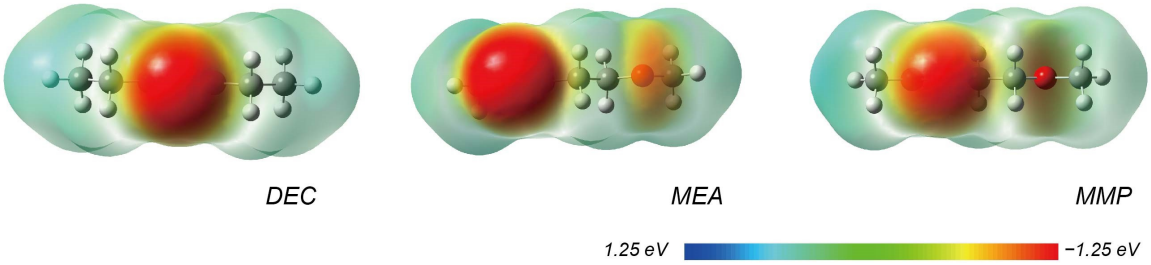

Figure S1. Electrostatic potentials of DEC, MEA, and MMP.

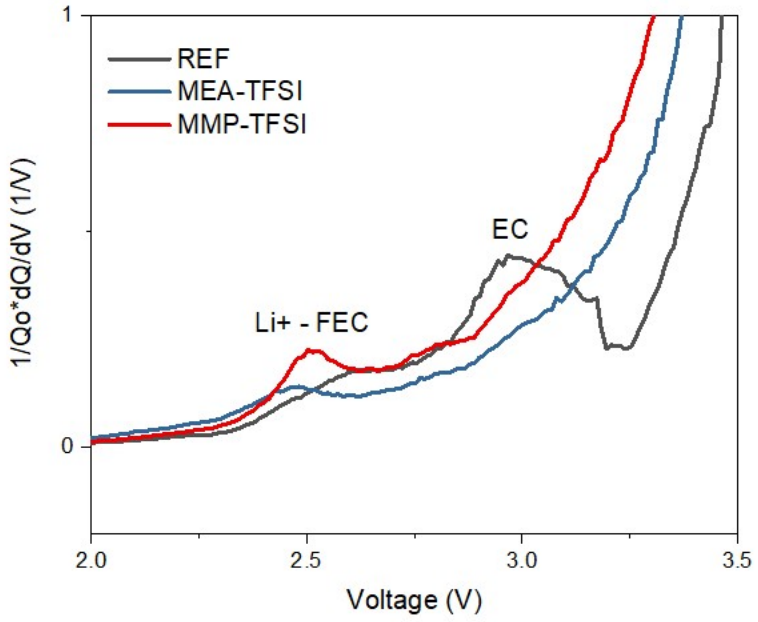

Figure S2. dQ/dV profiles of full cells with different electrolytes during the first charging.

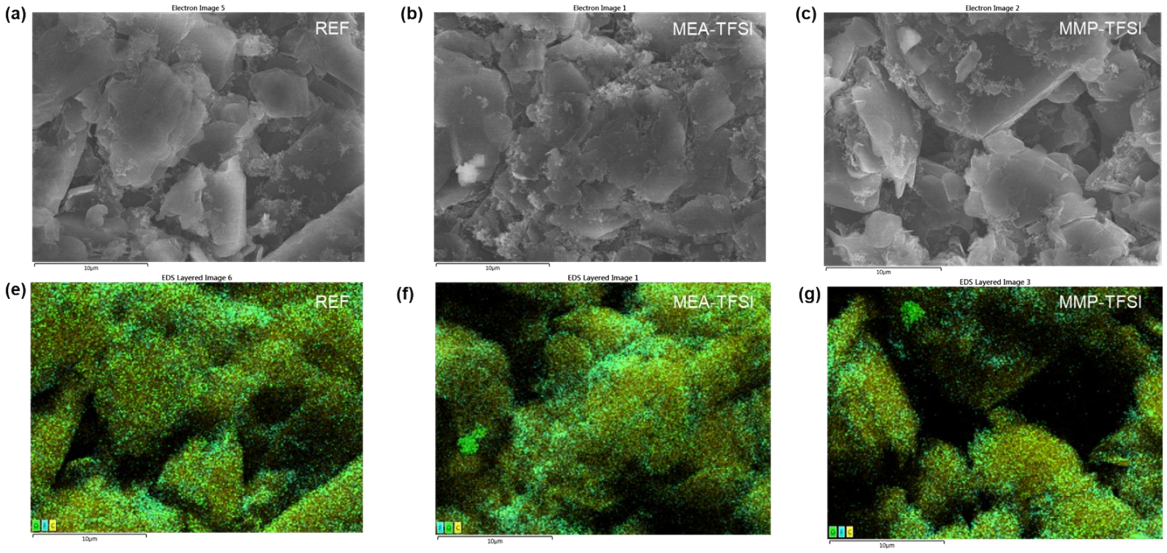

Figure S3. SEM images and EDS mapping of graphite anodes with (a, c) Ref, (b, f) MEA-TFSI, and (c, g) MMP-TFSI electrolytes after formation cycles.

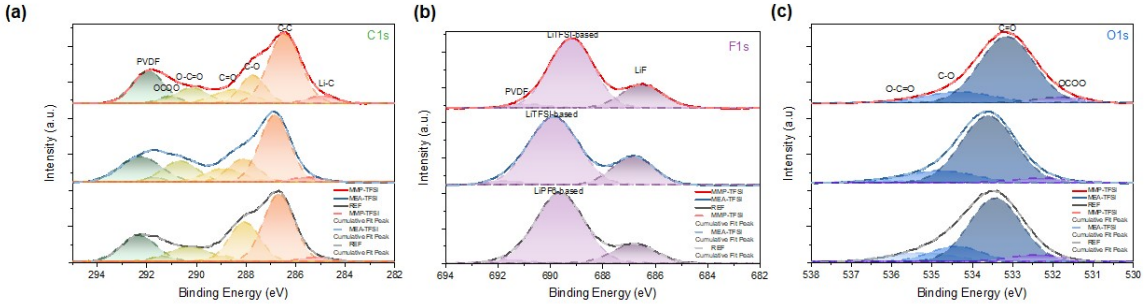

Figure S4. XPS spectra of graphite anodes with Ref, MEA-TFSI, and MMP-TFSI electrolytes after formation cycles in (a) C 1s, (b) F 1s, and (c) O 1s.

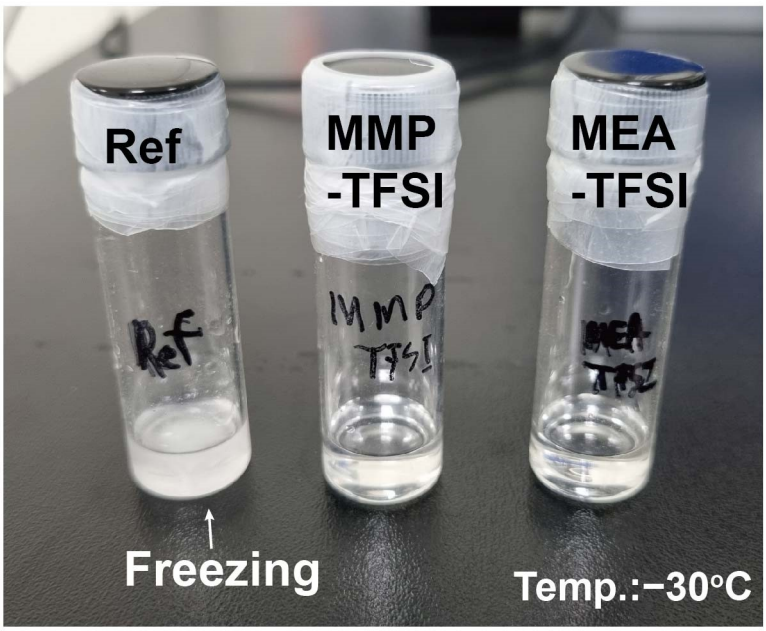

Figure S5. Optical image of Ref, MEA-TFSI, and MMP-TFSI electrolytes stored at −30°C.

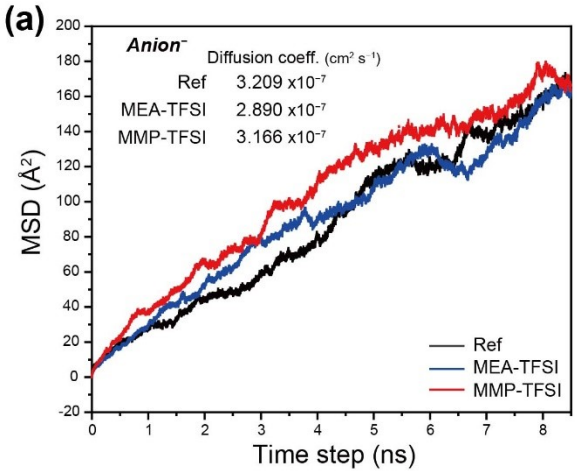

(b)

	Transference number (Li^+)
Ref	0.3542
MEA-TFSI	0.4183
MMP-TFSI	0.4184

Figure S6. (a) Mean square displacement (MSD) curves of anions and (b) calculated transference numbers in Ref, MEA-TFSI, and MMP-TFSI electrolytes.

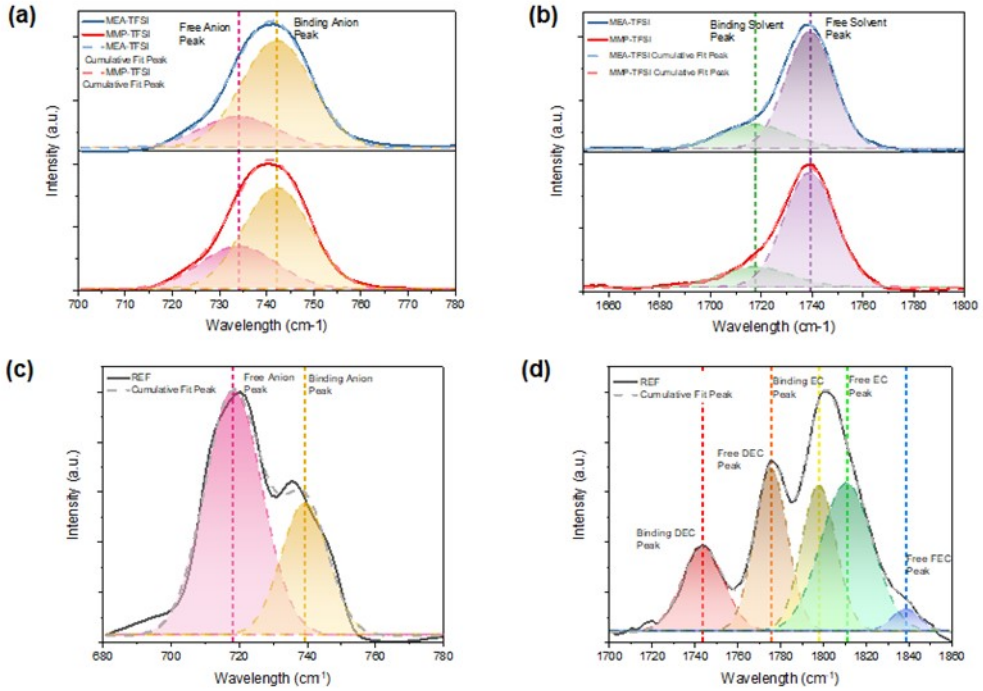

Figure S7. Raman spectra of Ref, MEA-TFSI, and MMP-TFSI electrolytes.

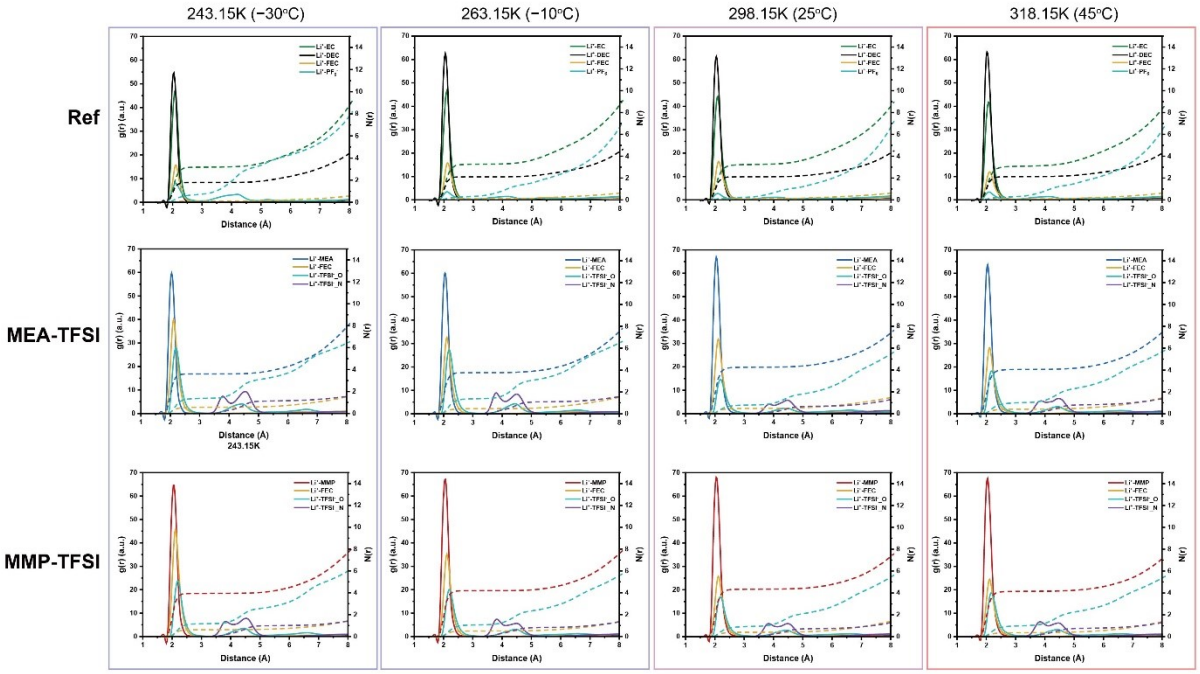

Figure S8. Radial distribution functions of Ref, MEA-TFSI, and MMP-TFSI electrolytes at various temperatures.

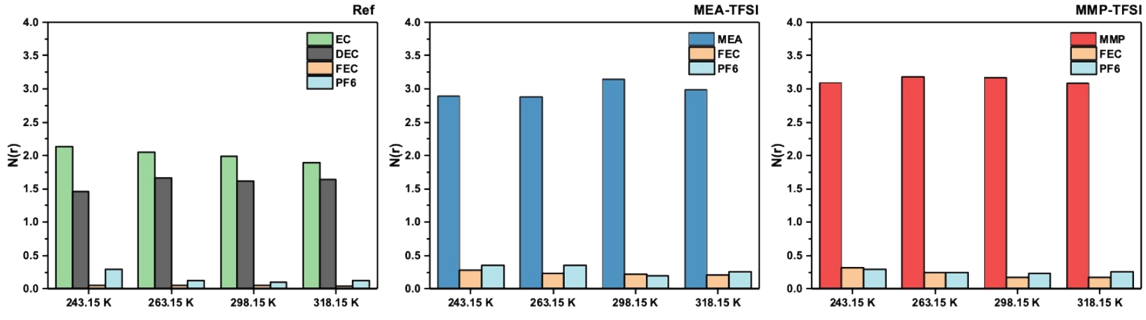

Figure S9. Coordination numbers as a function of temperature in EC/DEC, MEA, and MMP electrolytes.

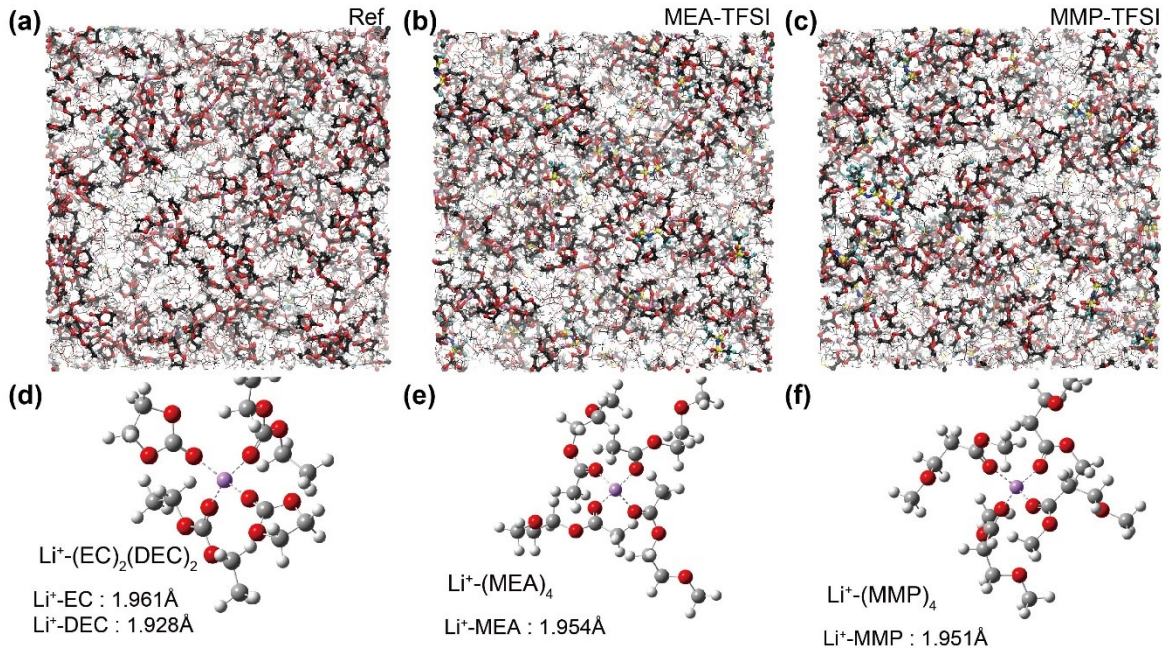

Figure S10. Snapshots of the MD simulations and representative solvation structures of (a, d) Ref, (b, e) MEA-TFSI, and (c, f) MMP-TFSI electrolytes.

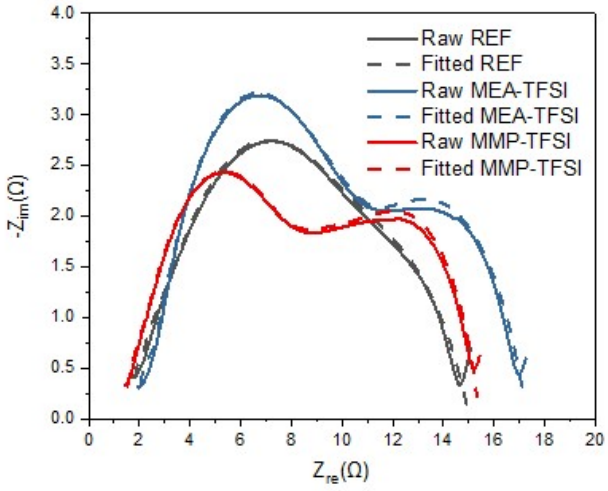

Figure S11. Nyquist plots and fitting results of Ref, MEA-TFSI, and MMP-TFSI electrolytes.

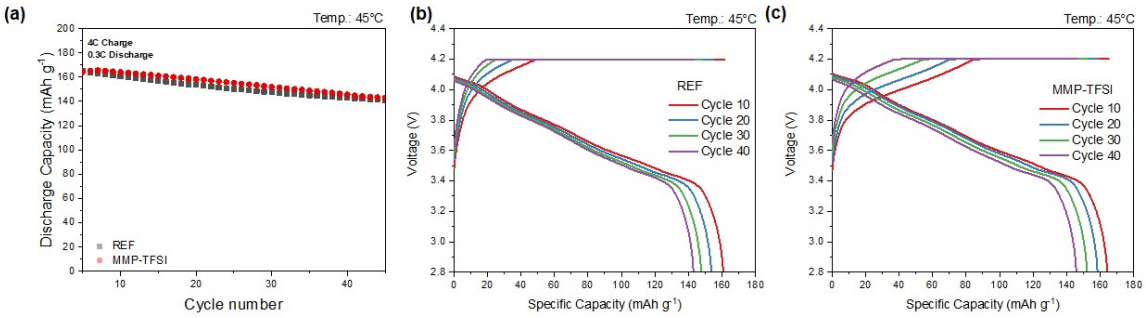

Figure S12. (a) Cycling performances and profiles of (b) Ref, and (c) MMP-TFSI electrolytes at 45°C.

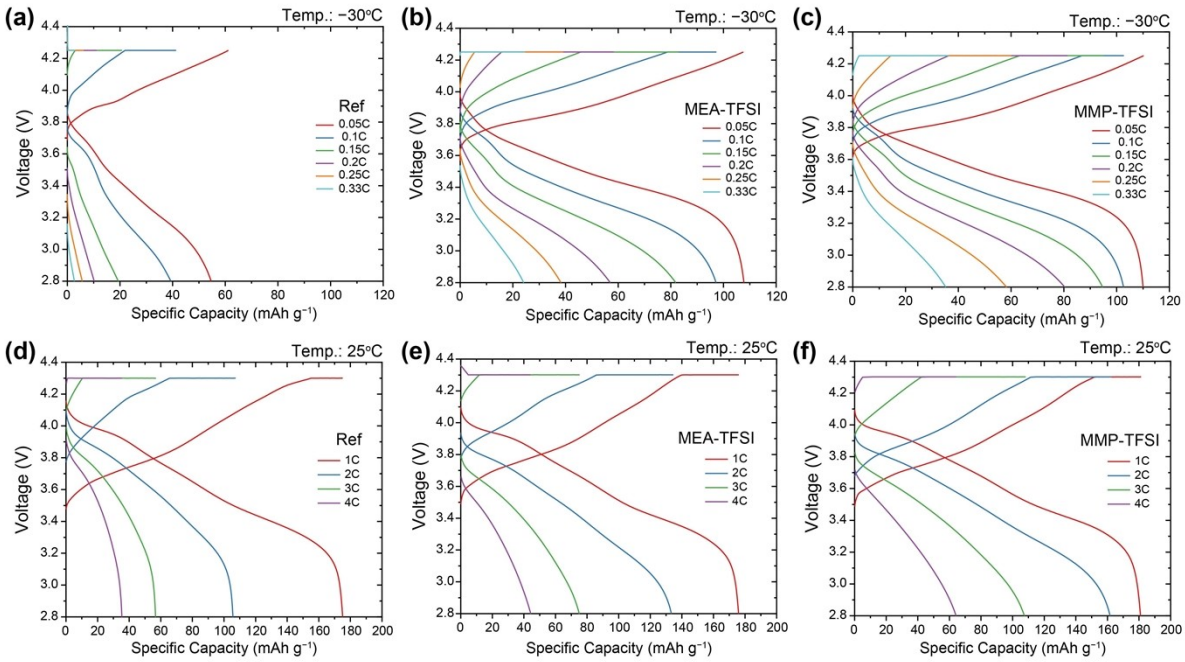

Figure S13. Voltage profiles of (a, d) Ref, (b, e) MEA-TFSI, and (c, f) MMP-TFSI electrolytes at −30°C and 25°C.

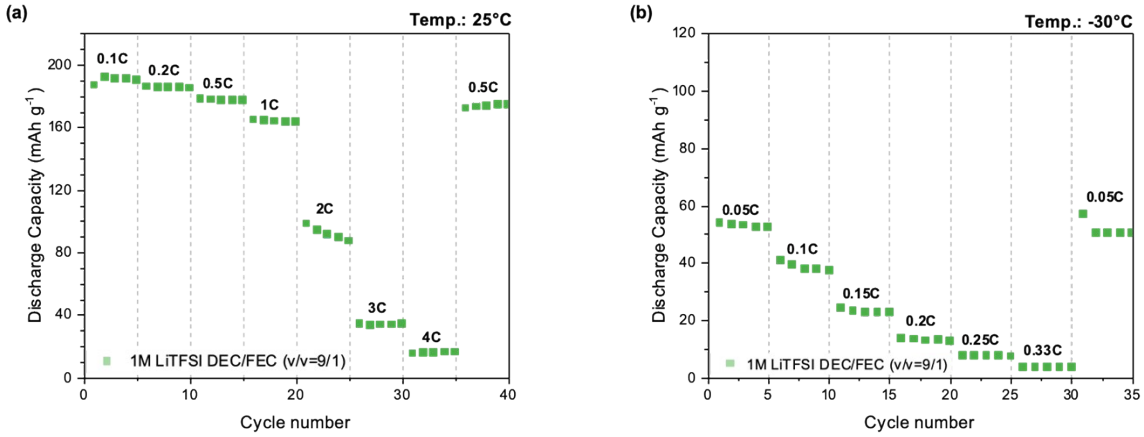

Figure S14. Rate capabilities of 1M LiTFSI DEC/FEC (v/v=9/1) at temperatures of (a) 25 °C and (b) -30°C.

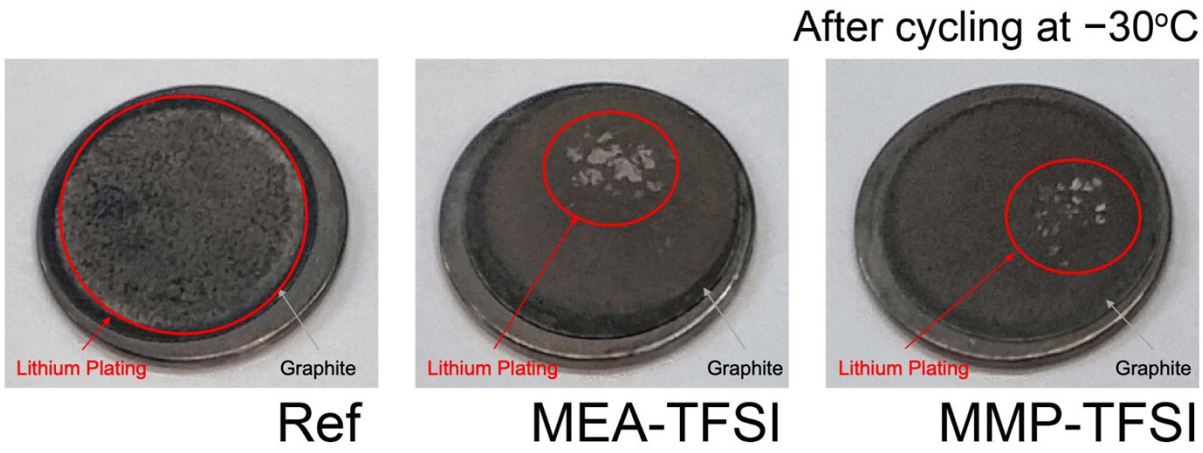

Figure S15. Image of graphite anodes with Ref, MEA-TFSI, and MMP-TFSI electrolytes after cycling at −30°C.

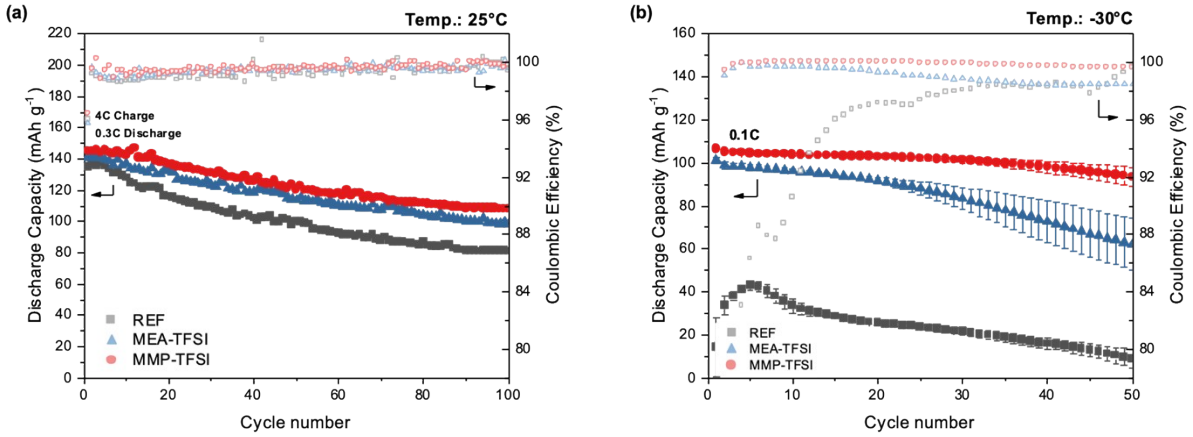

Figure S16. Cycling performances of REF, MEA-TFSI, and MMP-TFSI at temperatures of (a) 25 ^{o}C and (b) -30^{o}C with coulombic efficiency.

REFERENCES

(1) Kaminski, G. A.; Friesner, R. A.; Tirado-Rives, J.; Jorgensen, W. L. Evaluation and reparametrization of the OPLS-AA force field for proteins via comparison with accurate quantum chemical calculations on peptides. *The Journal of Physical Chemistry B* **2001**, *105* (28), 6474-6487.
(2) Jensen, K. P.; Jorgensen, W. L. Halide, ammonium, and alkali metal ion parameters for modeling aqueous solutions. *Journal of Chemical Theory and Computation* **2006**, *2* (6), 1499-1509.
(3) Doherty, B.; Zhong, X.; Gathiaka, S.; Li, B.; Acevedo, O. Revisiting OPLS force field parameters for ionic liquid simulations. *Journal of chemical theory and computation* **2017**, *13* (12), 6131-6145.
(4) Gouveia, A. S.; Bernardes, C. E.; Tomé, L. C.; Lozinskaya, E. I.; Vygodskii, Y. S.; Shaplov, A. S.; Lopes, J. N. C.; Marrucho, I. M. Ionic liquids with anions based on fluorosulfonyl derivatives: from asymmetrical substitutions to a consistent force field model. *Physical Chemistry Chemical Physics* **2017**, *19* (43), 29617-29624.
(5) Zhang, X.; Xu, P.; Duan, J.; Lin, X.; Sun, J.; Shi, W.; Xu, H.; Dou, W.; Zheng, Q.; Yuan, R.; et al. A dicarbonate solvent electrolyte for high performance 5 V-Class Lithium-based batteries. *Nature Communications* **2024**, *15* (1), 536. DOI: 10.1038/s41467-024-44858-3.
(6) Sambasivarao, S. V.; Acevedo, O. Development of OPLS-AA force field parameters for 68 unique ionic liquids. *Journal of chemical theory and computation* **2009**, *5* (4), 1038-1050.
(7) Martínez, L.; Andrade, R.; Birgin, E.; Packmol, J. M. A package for building initial configurations for molecular dynamics simulations., 2009, 30. *DOI: https://doi. org/10.1002/jcc 21224*, 2157-2164.
(8) Stephens, P. J.; Devlin, F. J.; Chabalowski, C. F.; Frisch, M. J. Ab initio calculation of vibrational absorption and circular dichroism spectra using density functional force fields. *The Journal of physical chemistry* **1994**, *98* (45), 11623-11627.
(9) Krishnan, R.; Binkley, J. S.; Seeger, R.; Pople, J. A. Self-consistent molecular orbital methods. XX. A basis set for correlated wave functions. *The Journal of chemical physics* **1980**, *72* (1), 650-654.
(10) Marenich, A. V.; Cramer, C. J.; Truhlar, D. G. Universal solvation model based on solute electron density and on a continuum model of the solvent defined by the bulk dielectric constant and atomic surface tensions. *The Journal of Physical Chemistry B* **2009**, *113* (18), 6378-6396.